Eur. Phys. J. B **14**, 773–781 (2000)

THE EUROPEAN PHYSICAL JOURNAL B

EDP Sciences

Controlling the Bénard-von Kármán instability in the wake of a cylinder by driving the pressure at the front stagnation point

R.H. Hernández[1], C. Baudet[1], and S. Fauve[2,a]

[1] Laboratoire de Physique[b], École Normale Supérieure de Lyon, 46 allée d'Italie, 69364 Lyon Cedex 07, France
[2] Laboratoire de Physique Statistique[c], École Normale Supérieure, 24 rue Lhomond, 75231 Paris Cedex 05, France

Received 2 August 1999

Abstract. We report an experimental method for inhibiting vortex shedding generated by the Bénard-von Kármán instability (BvK) in the wake of a cylinder. We show that monitoring the pressure at the front stagnation point of a circular cylinder can completely suppress the Bénard-von Kármán instability for Reynolds numbers in the range $48.5 < \mathrm{Re} < 150$. We then study some properties of the BvK instability in the presence of suction at the front stagnation point and mention that this method can be used to generate well-controlled localized vortical structures in the form of vortex pairs.

PACS. 47.20.-k Hydrodynamic stability – 47.27.Rc Turbulence control – 47.27.Vf Wakes

1 Introduction

It has been known since the early paper of Prandtl on boundary layers [1] that a small amount of suction on one side of a cylinder in a high Reynolds number flow, is enough to prevent the separation of the boundary layer on that side.

Almost a century later, the control of boundary layers or more generally of the hydrodynamical instabilities of the near wake past bluff bodies in high Reynolds number flows, is still a matter of central interest in fluid dynamics. The motivation is primarily to achieve drag reduction but also to prevent any structural damage of a bluff body resulting from a resonant coupling with the hydrodynamic instability in its near wake.

A phenomenon which generates strong transverse force fluctuations, and thus may be involved in such a coupling, is vortex shedding from bluff bodies. A widely studied canonical example is the Bénard-von Kármán (BvK) instability generated in the wake of a circular cylinder of diameter d and length L, such that the aspect ratio, $\Gamma = L/d \gg 1$. At Reynolds number of order one ($\mathrm{Re} = U_0 d/\nu$, where U_0 is the upstream velocity and ν is the kinematic viscosity of the fluid), a reversed flow first occurs near the rear stagnation point of the cylinder and leads to the formation of two attached eddies in the near wake of the cylinder, thus breaking the upstream-downstream symmetry. The two attached eddies grow in size as the Reynolds number is increased, and at a critical Reynolds number, $\mathrm{Re_c} \sim 48.5$, the flow ceases to be symmetric about the centerline and stationary; it settles into a time periodic regime in which vortices are shed alternatively from the two sides of the cylinder, so giving the von Kármán vortex street [2]. Vortex shedding corresponds to a limit-cycle oscillation of the near wake described by a Stuart-Landau equation [3].

Controlling the wake of a cylinder by inhibiting the BvK instability has motivated a lot of studies. Two forms of wake control are currently proposed in the literature, called respectively active or passive methods. In the group of passive methods, inserting a splitter plate in the near wake of a cylinder [4], performing steady or periodic suction from the rear re-circulation zone [5], heating the cylinder, locating a secondary cylinder in the near wake, imposing large-amplitude transverse oscillations or angular rotation to the cylinder at an appropriate frequency, can at least modify or suppress vortex shedding [6–8]. In the group of active methods, an electronic feedback is achieved with the aid of a pressure sensor, by applying for instance acoustic forcing [9,10] or using a pair of blowing-suction actuators near the re-circulation region [9].

Most of the above methods, active or passive, have tried to control the BvK instability by applying a local perturbation directly in the near wake of the cylinder. This is a quite natural idea if we have in mind the methods used to control boundary layer separation by trying to inhibit adverse pressure gradients along the trailing edge of solid bodies in a flow field. Another concept that may be invoked to justify a perturbation directly applied to the wake is the one of absolute *vs.* convective instability [11]; by perturbing the wake, for instance using a blowing actuator at the rear stagnation point, one may hope

[a] e-mail: fauve@physique.ens.fr
[b] CNRS, UMR 5672
[c] CNRS, UMR 8550

to transform an absolute instability of the near wake into a convective one.

We propose a method of control which differs from the ones mentioned above. We have tried to achieve a global modification of the flow field around the cylinder by monitoring the pressure distribution. In general, the average pressure in the near wake is smaller than the one near the front stagnation point. This important difference with the potential flow solution, is due to boundary layer separation that generates a vorticity filled wake in which the pressure is low. The general idea is thus to compensate this pressure difference by decreasing the pressure at the front stagnation point, say $\mathbf{r}_o$. This is achieved by a suction which decreases the pressure $p(\mathbf{r}_o, t)$. The front stagnation point is thus suppressed and bifurcates into a pair of stagnation points located symmetrically with respect to the flow centerline, at angles $\pm\theta_o$, and shifted downstream as the amount of suction is increased. We have shown using potential flow theory, that this modifies the pressure distribution around the whole cylinder such that the streamlines shrink in the wake of the cylinder. This externally imposed asymmetry is thus likely to compensate the one which results from boundary layer separation and consequently to delay the onset of the BvK instability.

This paper is organized as follows: in the next section, we describe the experimental apparatus and the measurement techniques. We then show that a suction at the front stagnation point of the cylinder does inhibit the BvK instability in Section 3. Section 4 is devoted to the study of the properties of the BvK instability in the presence of suction. In Section 5, we show that a simple model in the framework of potential flow theory gives insights in the inhibition mechanism. In the conclusion, we mention the use of the present technique to the generation of well-controlled vortical localized structures.

2 Experimental facilities and instrumentation

The experiments were conducted in a low velocity air wind tunnel at ENS-Lyon (Fig. 1). This open wind tunnel has a laminarisation chamber built of 4 metallic honey comb panels placed between the test section and the fans. A fine metallic grid (step 0.5 mm) is used to reduce transverse velocity fluctuations. The turbulence level, defined as the ratio of the rms axial velocity to the average axial velocity, does not exceeds 0.3% with accuracy better than $\pm 1\%$ on mean velocity. Indeed, a low fluctuation level is necessary to prevent a spurious amplification of the BvK instability due to the presence of uncontrolled free stream fluctuations.

At the center of the test section of 50×50 cm^2 and 2.5 m long, a vertical circular cylinder is mounted. The circular cylinder consists in brass tubes of external diameter $d = 3$ mm (respectively 5 mm) and length L with a constant aspect ratio $\Gamma = L/d = 56$. The vortex shedding process being extremely sensitive to boundary conditions, circular end-plates of diameter d_p (ratio $d_p/d = 12$), are mounted to limit the span L, more than

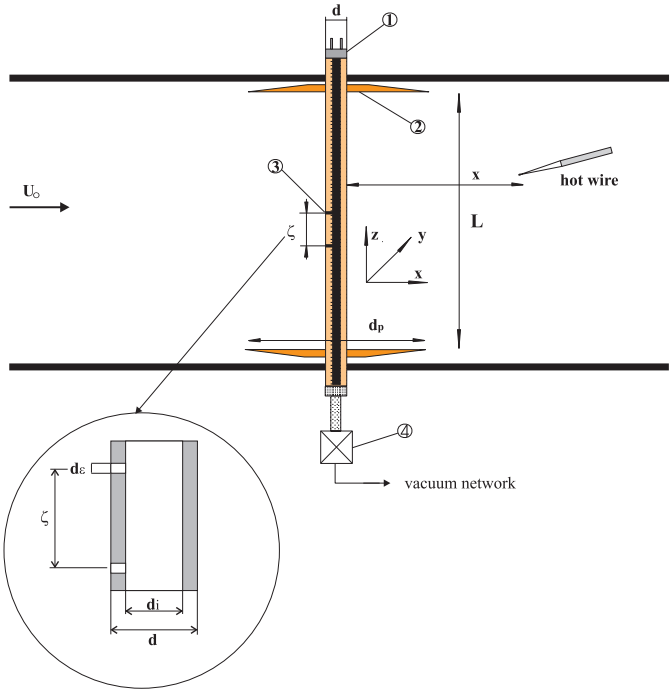

Fig. 1. Experimental set up. A vertical circular cylinder of diameter d and length L is mounted in the test section of the wind tunnel. (1) Pressure sensor. (2) Circular end-plate of diameter d_p. (3) Small hole distribution: hole diameter d_ϵ, step between holes ζ. (4) Control valve and flow meter.

50 cylinder diameters apart to avoid the presence of other shedding modes [12]. The Reynolds number is in the range $50 < \mathrm{Re} < 150$.

Local wake-velocity measurements are performed with a calibrated TSI hot film probe TSI-1240-20, 51 μm in diameter and 1 mm long sensitive length. The hot film is located at $x/d = 37.8$ from the rear end of the cylinder in the case of $d = 3$ mm, and at $x/d = 24.5$ in the case of $d = 5$ mm. It is operated with a TSI 1750 constant temperature anemometer. The signal delivered by the anemometer is maximum in amplitude when the probe is located slightly off the center of the wake at $y/d = 1.75$ (Fig. 1).

In order to decrease the pressure at the stagnation point, $p(\mathbf{r}_o, t)$, we have drilled a very small hole of diameter d_ϵ ($d_\epsilon \ll d$) to connect the surface of the tube to its inner section where an internal pressure level $p_i(t)$ is imposed through an external vacuum pump (Fig. 1). To get an overall effect along the cylinder span L, we have drilled a uniform distribution of small holes along a straight line at the cylinder surface. To find an optimum step size between the holes, ζ, we performed experiments with one hole and looked at its maximum influence over the cylinder span with different combinations of the parameters: d_ϵ, d, $p(\mathbf{r}_o, t)$ and U_o. We have chosen a discrete hole distribution instead of a continuous slit because pressure modulation would not have been possible due to the limited power of the vacuum network at our disposal. We have studied three configurations differing only in the external diameter d of the circular cylinder and in the hole

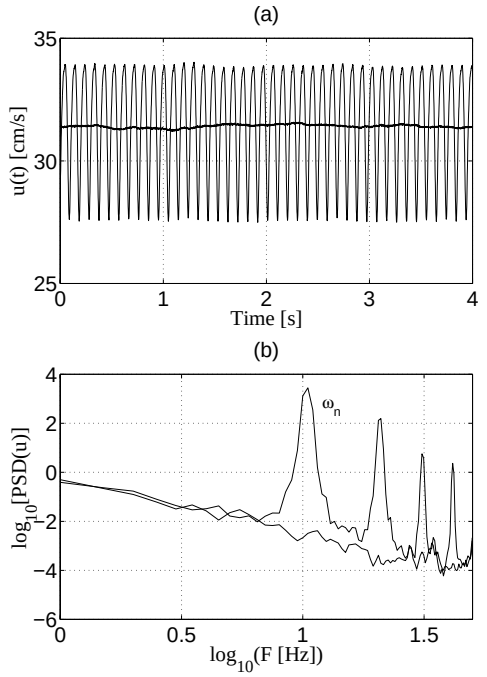

Fig. 2. (a) Time recording of the velocity fluctuations due to periodic vortex shedding in the free wake (thin line). Suppression of the oscillation when the pressure p_i is decreased inside the cylinder (thick line). (b) Power spectra corresponding to the time recordings of Figure 2a. $d = 5$ mm, $d_\epsilon = 0.5$ mm, Re = 116.

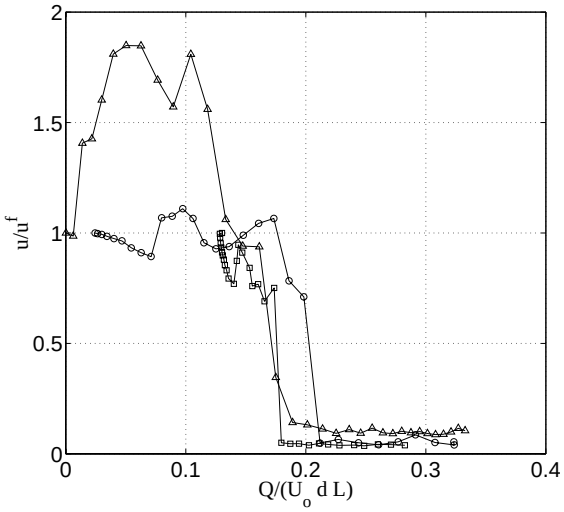

Fig. 3. Velocity fluctuations in the wake of the cylinder as a function of the overall flow rate Q. u/u^f *versus* $Q/(U_o dL)$ for: Re = 95.5, $d = 3$ mm, $d_\epsilon = 0.5$ mm (△), Re = 95.9, $d = 5$ mm, $d_\epsilon = 0.5$ mm (○) and Re = 94.5, $d = 3$ mm, $d_\epsilon = 0.3$ mm (□).

diameter d_ϵ: $d = 3$ mm, $d_\epsilon = 0.3$ mm, $d = 3$ mm, $d_\epsilon = 0.5$ mm, $d = 5$ mm, $d_\epsilon = 0.5$ mm. In all cases, $\zeta/d = 3.4$.

The applied pressure p_i, relative to the atmospheric pressure, is measured with a precision temperature-compensated differential pressure transducer Sensym SCX01-DN connected at one end of the cylindrical tube (operating range 0–1 psi, precision ±0.2% of full span). Pressure level is controlled with an electronically commanded valve which allows to apply pressure steps smaller than the precision of the pressure transducer. Alternatively, rapid pressure changes can be performed by means of a solenoid on-off valve. The total flow rate Q is measured with calibrated flow meters Brooks R215C and R615B. Velocity as well as pressure signals are simultaneously digitized by a 16 bit 50.2 kHz HP3565 input module.

3 The inhibition of the Bénard-von Kármán instability

We start with the free wake at Re = 116. A time recording of velocity fluctuations is displayed in Figure 2a showing the oscillations associated to the periodic vortex shedding. The pressure p_i inside the cylinder is then decreased in a quasistatic way, *i.e.* by steps of order $\delta p_i \sim 4$ pa, with a waiting time 30 seconds between each step. Below a critical pressure p_{ic}, the oscillation disappears and the rms velocity signal falls down to the background velocity fluctuation level of the mean stream (Fig. 2a), indicating that vortex shedding has been suppressed. We emphasize that vortex shedding suppression has been confirmed through velocity measurements performed on the whole transverse section of the flow. Thus, our observation does not result from a simple wake deflection. We also note from Figure 2a that the mean velocity measured in the wake is not significantly decreased by the applied suction.

In the whole range of Reynolds numbers investigated here ($50 < \mathrm{Re} < 150$), we have shown that the suppression of vortex shedding, *i.e.* the control of the BvK instability, is achieved by decreasing the value of the internal pressure p_i below a critical one p_{ic} which corresponds to a critical flow rate Q_c entering the cylinder.

The rms values of velocity fluctuations as a function of p_i, $u(p_i)$, normalized by the free wake velocity, u^f, as a function of the flow rate, Q, normalized by $U_o dL$, are displayed in Figure 3. For three d/d_ϵ ratios, one observes a transition at which the velocity fluctuations fall into the background fluctuation level, revealing that vortex suppression occurs. Although the transition is rather abrupt, no hysteresis is detectable. The method to determine critical values for pressure, p_{ic}, and critical total flow rate, Q_c, will be discussed later.

Different regimes are identified from the behavior of rms velocity fluctuations as the pressure, p_i, is decreased or the flow rate, Q, increased (Fig. 4b). First there is a nearly monotonous decrease of the amplitude of the velocity fluctuations at a constant frequency ω_n; then a shift to a lower frequency mode ω_s but with an increase of the fluctuation amplitude. ω_s also remains constant as Q is increased further until the suppression of the vortex shedding is observed (Fig. 4). For $100 < \mathrm{Re} < 150$, the reduced shift $(\omega_n - \omega_s)/\omega_n$ was found to be nearly constant roughly equal to 0.34.

Before studying the BvK instability in the presence of suction, let us consider the effect of only one suction hole

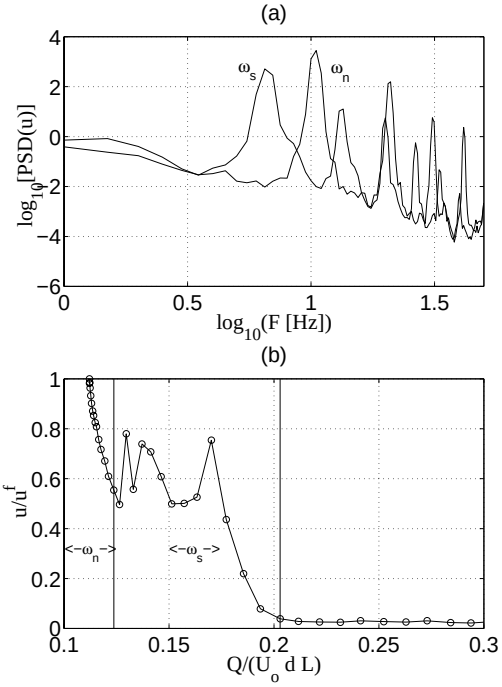

Fig. 4. (a) Power spectral density of wake velocity showing natural ω_n and slower ω_s modes for $d = 5$, $d_\epsilon = 0.5$ mm, Re = 109.4. (b) Velocity fluctuations u/u^f *versus* flow rate $Q/U_o dL$, and the regions where ω_n, ω_s exist.

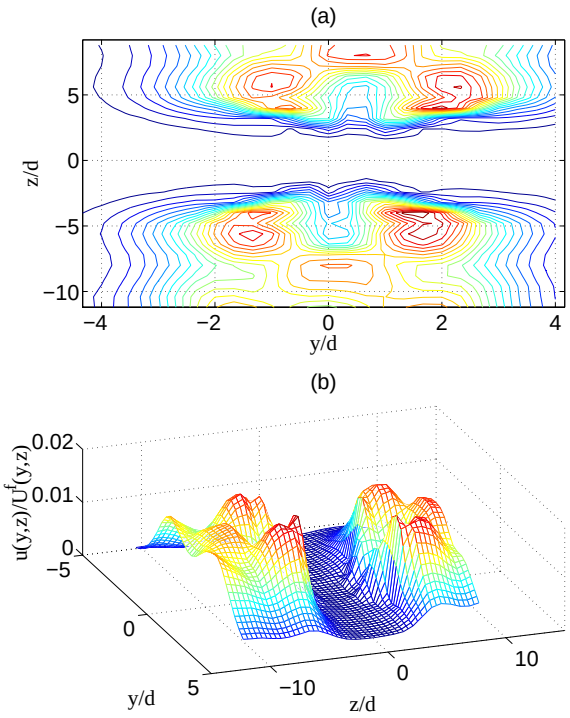

Fig. 5. The influence of a single sink. Surface plot and contours for the rms velocity profiles downstream around $\mathbf{r}_o$ *versus* x/d and y/d at Re = 82.5, $Q = 25.6$ cm^3/s. (a) Iso-contours of u/U^f for $d = 3$, $d_\epsilon = 0.5$ mm. (b) The corresponding surface plot of u/U^f for $d = 3$, $d_\epsilon = 0.5$. Note that U^f is the free mean velocity.

drilled in the cylinder, in order to determine the spanwise scale on which vortex shedding suppression is found around the sink point $\mathbf{r}_o$. We measure the velocity field around $\mathbf{r}_o$ scanning a whole downstream transverse plane (z–y) parallel to the cylinder axis. Figure 5 shows the contours and surface plots of the normalized rms velocity, $u(y, z)$ at $x/d = 11.3$ downstream from the cylinder rear end, for Re = 82.5, $d = 3.5$ mm and $d_\epsilon = 0.5$ mm. Vortex suppression takes places along the span around $\mathbf{r}_o$ giving a spatial scale of $|z/d| \sim 4$ for $d = 3$ mm (respectively 5 mm). This determined our choice for the ζ/d ratio. Note that a decrease of ζ/d will require smaller values of the depression in order to obtain the same effect along the span. However the total section associated to N holes distribution $\sum_{i=1}^{N}(\pi d_\epsilon^2/4)$ will require a net increase in terms of the flow rate because the BvK instability inhibition is caused by the strength of each sink, its local flow rate q, where $Q = Nq$.

4 The Bénard-von Kármán instability in the presence of suction

The critical value of the internal pressure, p_{ic} as well as the critical flow rate Q_c at which the suppression of vortex shedding occurs, depend on the upstream velocity U_o. In this section we determine this experimental relationship.

Critical pressure can be obtained from the quasistatic curves. But it is known to be more accurate to obtain p_{ic} from an extrapolation of the linear fit of the relation giving the temporal growth rate, σ_r, of the natural shedding mode *versus* the internal pressure, p_i. σ_r is found from the initial exponential growth of the velocity signal at the first stage of the instability growth. We operate as follows: for a fixed value of Re, Re > Re$_c$, we apply an internal pressure that suppresses the instability, p_i^1, so the pressure is below the critical one, $p_i^1 < p_{ic}$. Then, we increase p_i impulsively with a control valve to reach a supercritical level, $p_i^2 > p_{ic}$. The time scale, τ, on which the pressure is varied from $p_i^1 \to p_i^2$, must be smaller than the inverse of the instability growth rate, *i.e.*, $\tau \ll \sigma_r^{-1}$, otherwise a phenomenon of amplitude modulation of the natural mode takes place due to a coupling with the forcing pressure. Figure 6 shows a typical evolution of the instability when we perform a rapid transition from $p_i^1 \to p_i^2$ (Re = 53.6). The time series of the normalized velocity fluctuation, $u(t)/u^{sat}$ (at $x/d = 37.8$ and $y/d = 1.75$) displays an exponential growth followed by a nonlinear saturation. The forcing pressure signal $p_i(t)$ displays a time lag with respect to the velocity signal because data acquisition is performed simultaneously (synchronized) and the velocity is measured downstream from the cylinder.

Figure 7 shows that the extrapolation of the linear fit of σ_r *versus* p_i gives the critical value p_{ic} and the corresponding critical flow rate Q_c. This works well because the growing time scale of the instability diverges when we approach the critical value, *i.e.*, $1/\sigma_r \to \infty$ as $p_i \to p_{ic}$ similarly to other experiments on the BvK

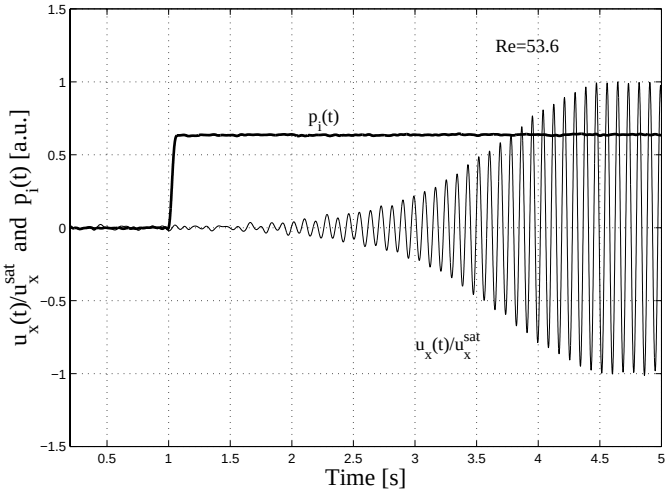

Fig. 6. Typical wake velocity recording of the Bénard-von Kármán instability, $u(t)/u^{\rm sat}$, and the associated normalized vacuum pressure, $p_{\rm i}(t)$, for Re = 53.6, $d = 3$, $d_\epsilon = 0.5$ mm.

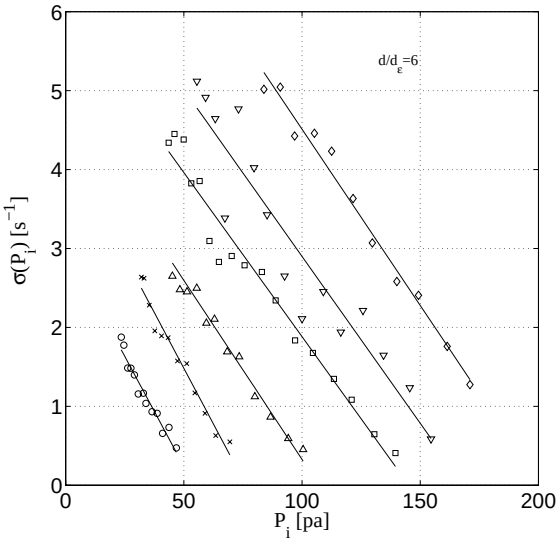

Fig. 7. Growth rates, $\sigma_{\rm r}$, for the Bénard-von Kármán instability *versus* the applied pressure, $p_{\rm i}$, for $d = 3$, $d_\epsilon = 0.5$ mm. Best linear fit extrapolated to 0, $\sigma_{\rm r} \to 0$, gives an accurate value of the critical pressure, $p_{\rm ic}$. Re = 53.6 (○), 57.6 (×), 61.2 (△), 65.6 (□), 69.6 (▽), 72.4 (◇).

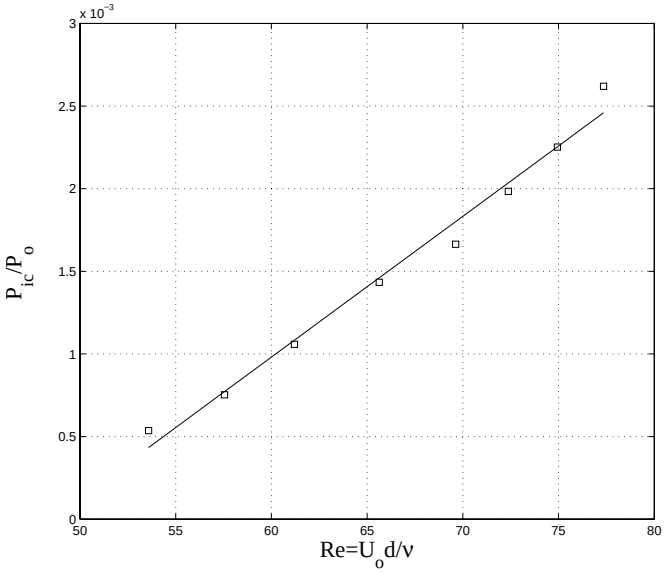

Fig. 8. Critical pressure $p_{\rm ic}$ ($p_{\rm o}$ is atmospheric pressure) as a function of the Reynolds number $\mathrm{Re} = U_{\rm o} d/\nu$ using the curves of Figure 7, for $d = 3$, $d_\epsilon = 0.5$ (□) mm and the linear fit (full line).

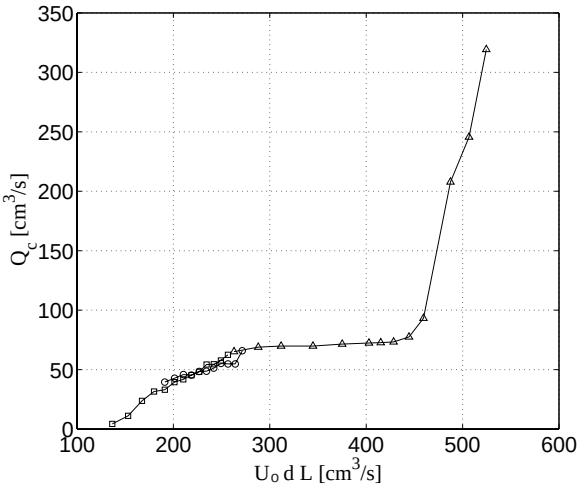

Fig. 9. Total critical flow rate $Q_{\rm c}$ as a function of the parameter $U_{\rm o} dL$, for $d = 3$, $d_\epsilon = 0.3$ mm (○), $d = 3$, $d_\epsilon = 0.5$ mm (□), $d = 5$, $d_\epsilon = 0.5$ mm (△).

instability where the Reynolds number is the control parameter [13,3]. This method works fine for Reynolds numbers below 100, because as Re increases, the growth rate become larger, and the condition $\tau \ll \sigma_{\rm r}^{-1}$ is no longer fulfilled. For Reynolds numbers above 100 we are forced to use an artificial threshold cutoff to determine the critical parameters damping the BvK instability. At each Re the cutoff is given by the rms background velocity fluctuation level. So $p_{\rm ic}$, $Q_{\rm c}$ are found intersecting a local linear fit of $u(p_{\rm i})$ with this cutoff. This method is less accurate but also works well.

Figure 8 shows that the normalized critical pressure grows linearly with the Reynolds number. Note that the critical Reynolds number, $\mathrm{Re}_{\rm c}$, for the BvK instability, can be evaluated by taking the limit $p_{\rm ic} \to 0$. We computed this limit by extrapolating a linear fit of Re *versus* $p_{\rm ic}$ for the case $d = 3$, $d_\epsilon = 0.5$ mm and we found $\mathrm{Re}_{\rm c} = 48.5$ which is now the more widely accepted value for the critical Reynolds number [14]. For the other cases it has not been possible to reach neither slower mean stream velocities (case $d = 5$, $d_\epsilon = 0.5$ mm) nor very small sink flow rates (case $d = 3$, $d_\epsilon = 0.3$ mm) to explore this limit.

Figure 9 displays the evolution of the total critical flow rate $Q_{\rm c}$ as a function of the flow rate $U_{\rm o} dL$ which seems to be the appropriate parameter to display the overall behavior of critical parameters for the three cases we

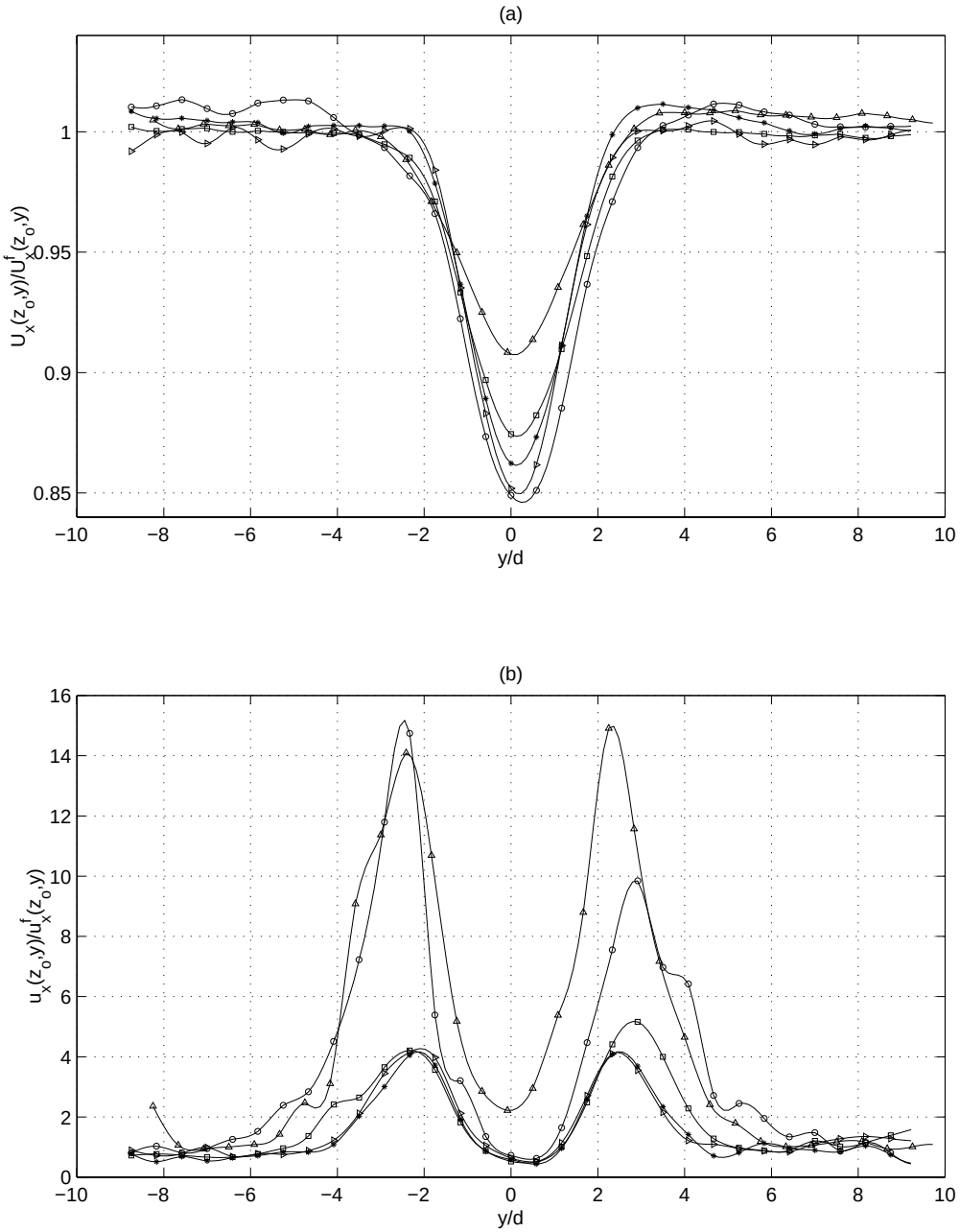

Fig. 10. Ratio of free/forced (a) mean velocity profiles, $U(z_o, y)/U^f(z_o, y)$, (b) rms fluctuating velocity, $u_x(z_o, y)/u^f_x(z_o, y)$, behind the circular cylinder ($x/d = 45.5$, $d/d_\epsilon = 6$, $Q = 400$ cm^3/s) at Re = 66.4 (○), Re = 74.3 (△), Re = 82.5 (□), Re = 89.8 (⋆) and Re = 96.6 (▷).

investigated ($d = 3$, $d_\epsilon = 0.3, 0.5$ mm and $d = 5$, $d_\epsilon = 0.5$ mm). The critical flow rate, Q_c, shows a slow increase between Re = $(50, 110)$ followed by an abrupt increase at higher Re that tends to show that the inhibition of the BvK instability is more and more difficult to achieve.

Figure 10a shows velocity profiles at different Reynolds numbers. The total flow rate is fixed $Q \sim 400$ cm^3/s. The mean velocity is systematically increased behind the cylinder when suction is active. This is an indicator that vortex shedding has ceased which is consistent with the decrease of velocity fluctuations in Figure 10b.

5 Discussion

We performed smoke-wire visualizations to show the influence on the velocity field of a sink at the front stagnation point of the cylinder. A smoke-wire generator is placed upstream from the cylinder ($x/d > 10$) intersecting a sheet of laser light perpendicular to the cylinder axis.

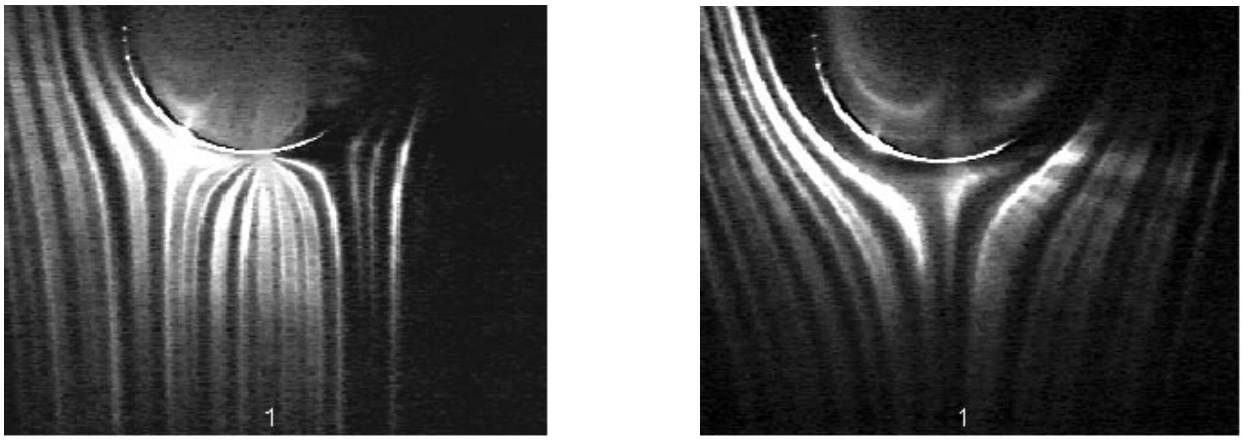

Slide 1 Slide 2

Fig. 11. Smoke-wire visualization of the stream lines upstream of a circular cylinder at Re = 200, $d = 18$, $d_\epsilon = 0.7$ mm. When the sink is on (slide 1) two stagnation points appear around the original one. The experimental angle, $\theta_\mathrm{o} \sim 160\,^\circ$, agrees well with the analytical estimation given by potential theory. When the sink is off (slide 2) the original stagnation point is recovered.

Figure 11 (Re = 200, $d = 18$, $d_\epsilon = 0.7$ mm) illustrates how the stream lines are deflected towards an active small hole (sink). Two new stagnation points are formed symmetrically around the original one at $\theta_\mathrm{o} \sim 160\,^\circ$ (slide 1, $q \sim 18$ cm^3/s). The experimental angle agrees well with the analytical estimation given by equation (1) (see below). The stream lines when the sink is off are shown in slide 2.

Figure 12a shows the effect of an active sink both on the boundary layer separation point and on the width of the cylinder wake (re-circulation region). Boundary layer separation is shifted downstream when the sink is active (slide 2) and one also observes a decrease of the width of the wake (Re = 119, $d = 8$, $d_\epsilon = 0.5$ mm).

Figure 12b shows a temporal sequence of three slides displaying the entire flow field around the cylinder when the strength of the sink is decreased (Re = 110, $d = 18$, $d_\epsilon = 0.5$ mm). We see a clear transition from a thin near wake when the sink is active (slide 1) to a wider one when the sink is off (slides 2 and 3).

The mechanism by which the vortex shedding is suppressed is related to the bifurcation of the original stagnation point into two points located at angles $\pm\theta_\mathrm{o}$ around cylinder axis. These new stagnation points appear as a consequence of the deflected fluid path produced by the active sink at $\mathbf{r}_\mathrm{o}$. The flow field created around one of the small holes at the cylinder surface can be modeled as a sink, *i.e.* by a potential of the form $\phi = q/(4\pi r)$ where q is the flow rate and r the radius from the hole center. A very simple model of the flow past a cylinder can be drawn from potential flow theory. If we superimpose the stream functions of a uniform flow, U_o, with a dipole of strength μ_d, we obtain the well-known overall flow around a circular cylinder. If we add a sink at the cylinder surface and a source somewhere inside the cylinder in order to maintain a constant value of the steam function on the cylinder, the stream function in cylindrical coordinates becomes,

$$\Psi(r,\theta) = U_\mathrm{o} r \sin(\theta) - \frac{\mu_\mathrm{d}}{2\pi r}\sin(\theta) + \frac{q_1}{2\pi}\theta' + \frac{q_2}{2\pi}\theta,$$

where a sink, q_1, is placed at $(r,\theta) = (R,\pi)$, $(\tan\theta' = y/(x+R))$ and a source, q_2, at $r = 0$. The cylinder radius, R, is given by $R = [(\mu_\mathrm{d}/(2\pi U_\mathrm{o})]^{1/2}$. The sink/source strength ratio found to retain the cylindrical shape is $|q_1/q_2| = 2$. A plot of the singular contour line, $\Psi(r,\theta) = 0$, shows that the initial stagnation point is shifted downstream symmetrically around $\theta = \pi$ (Fig. 13). Fluid particles coming from the left are pushed into the sink by a force which is proportional to both the free stream velocity, U_o and to the strength of the sink, q_1. This force vanishes precisely over the surface formed by the singular contour line. The position θ_o of the new stagnation points is determined through the pressure coefficient $C_\mathrm{p}(r,\theta) = 2\big(p(\theta) - p_\mathrm{o}\big)/\rho U_\mathrm{o}^2$ by the condition $C_\mathrm{p}(R,\theta) = 1$:

$$\theta_\mathrm{o} = \pm\cos^{-1}\left(\frac{q_1}{8\pi R U_\mathrm{o}} - 1\right). \qquad (1)$$

This shows that the original stagnation point at $\mathbf{r}_\mathrm{o}$ or $\theta = \pi$ bifurcates into two symmetric points at $\pm\theta_\mathrm{o}$. In the limit $q_1 \to 0, \theta_\mathrm{o} \to \pi$, the classical flow around the cylinder is recovered. The singular stream line $\Psi = 0$ which passes through these points, defines the boundary between fluid particles being sucked and those passing around the surface of the cylinder. At constant U_o, if the strength of the sink increases, the new stagnation points move downstream. As the boundary layer starts now at $\pm\theta_\mathrm{o}$, its separation point is also shifted downstream, thus reducing the size of the fluid loops behind the cylinder and inhibiting the BvK instability.

Equation (1) gives the correct order of magnitude for the shift of the stagnation point and potential flow theory thus roughly describes what happens in the experiment. The presence of a sink at the front end of a cylinder deflects the fluids paths creating an increased pressure field

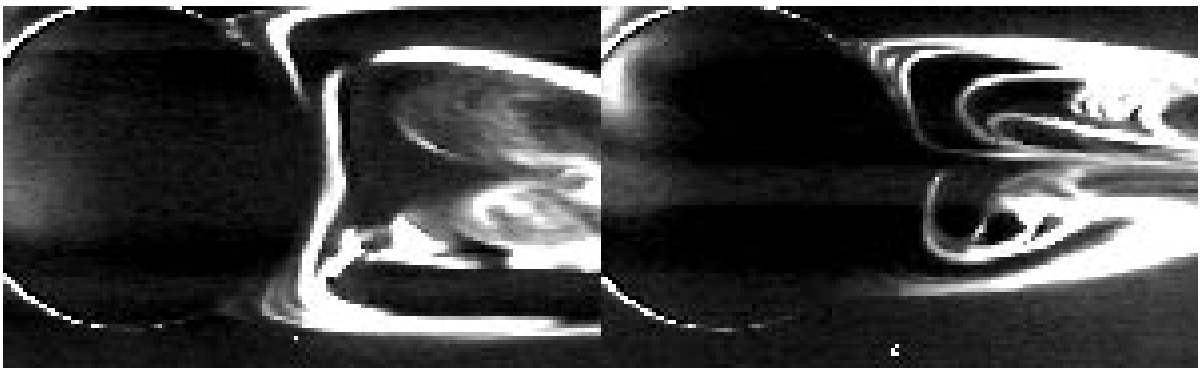

(a)

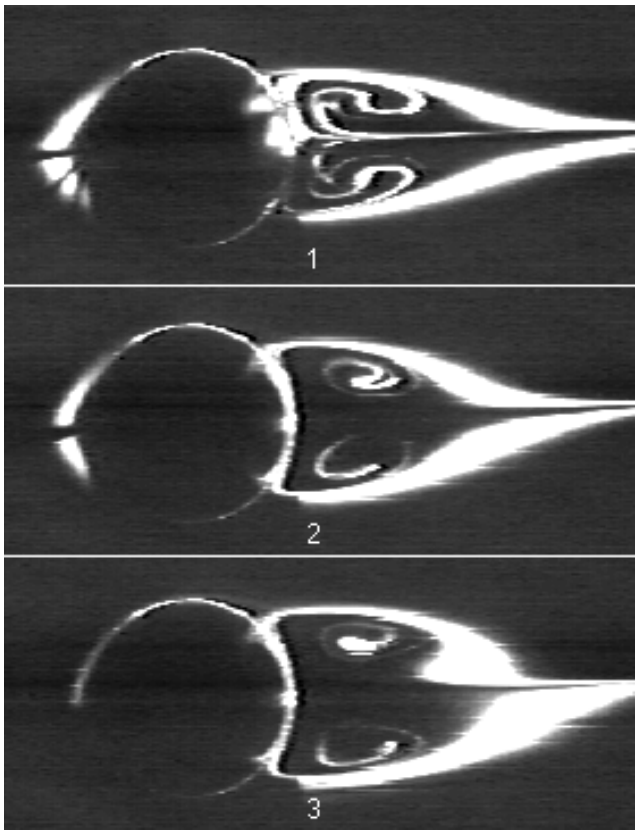

(b)

Fig. 12. (a) Smoke-wire visualization of the free and forced stream lines around a circular cylinder at Re = 110, $d = 8$, $d_\epsilon = 0.5$ mm. Slides 1 and 2 show the increased and reduced size of the re-circulation region behind the cylinder, and the breaking point of the boundary layer, for the free and forced case respectively. The individual strength of the sinks, q, is about 10 cm^3/s. (b) Smoke-wire visualization of the stream lines around a circular cylinder at Re = 110, $d = 8$, $d_\epsilon = 0.5$ mm, in the plane of a sink starting from a forced to free situation (slides $1 \rightarrow 3$). Note the reduced transverse size but increased longitudinal size of the re-circulation region in the forced case (slide 1).

around the cylinder. This compresses the re-circulating region behind the cylinder thus inhibiting the Bénard von Kármán instability and vortex shedding.

We know that a decrease of the width of the wake is followed by an overall drag reduction over the body. Indeed, the drag is approximately given by the integral of the streamwise velocity fluctuations across the wake [15],

$$F_x \simeq -\rho U_\mathrm{o} \iint u_x \mathrm{d}y\mathrm{d}z.$$

In Figure 10 we have shown the ratio between free/forced velocity profiles behind the circular cylinder. We can, in principle, integrate numerically across the wake, for

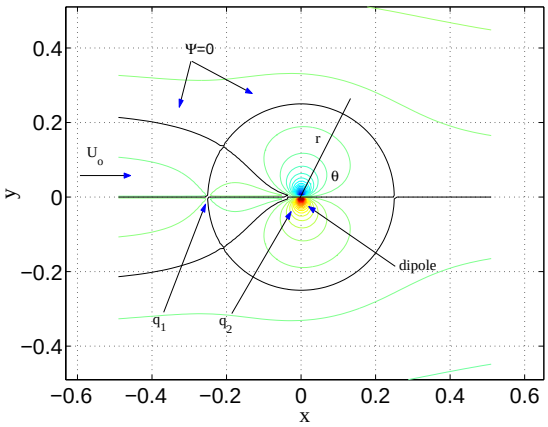

Fig. 13. Potential flow theory. Example of the stream function, $\Psi(r,\theta)$, for the flow around a circular cylinder with a sink, q_1 at $(r,\theta) = (R,\pi)$ and a source q_2 at $r = 0$. $\Psi(r,\theta) = U_o r\sin(\theta) - \frac{\mu_d}{2\pi r}\sin(\theta) + \frac{q_1}{2\pi}\theta' + \frac{q_2}{2\pi}\theta$, where $|q_1/q_2| = 2$. The two stagnation points at the cylinder surface deflect the fluid particles increasing the pressure gradient downstream which compresses the stream lines at the rear of the cylinder.

an unitary z step, to get approximately the percentage of drag reduction for a fixed value of sink flow rate q. We found a nearly constant 50 % drag reduction for $66 < \mathrm{Re} < 96.6$ due to a decrease of both the wake width and velocity, when the sinks are active ($Q \sim 400$ cm^3/s).

6 Conclusion

We have demonstrated an efficient method for controlling the Bénard-von Kármán instability in the wake of a cylinder thus suppressing vortex shedding by decreasing the pressure at the front stagnation point of the cylinder. Vortex suppression has been observed over a wide range of Reynolds numbers, $48.5 < \mathrm{Re} < 150$, thus improving previous methods used for controlling the wake of the cylinder [5,9,16].

The physical mechanism is associated to the bifurcation of the stagnation point into two points located symmetrically with respect to the flow centerline, and shifted downstream as the suction is increased. Their presence generates deflected fluid paths and an increased pressure field at the cylinder surface. This shrinks the streamlines in the near wake thus inhibiting vortex shedding. A corresponding drag reduction close to 50% is found for Re between 60–100 in the case $d/d_\epsilon = 6$.

By stopping the suction for a small enough duration in the supercritical regime, we are able to trigger the emission of only one pair of vortices. This method of control of the wake of a cylinder thus can be used to generate localized vortical structures in a well-controlled way.

This work has been partly supported by contract ECOS C98E04.

References

1. L. Prandtl, *Verhandlungen des III Internationalen Mathematiker Kongresses* (Heidelberg, 1904; Leipzig, 1905), p. 484.
2. see for instance, G.K. Batchelor, *An Introduction to Fluid Mechanics* (Cambridge University Press, 1967).
3. M. Provansal, C. Mathis, L. Boyer, J. Fluid Mech. **182**, 1 (1987).
4. K. Kwon, H. Choi, Phys. Fluids **8**, 479 (1996).
5. D.S. Park, D.M. Ladd, E.W. Hendricks, Phys. Fluids **6**, 2390 (1994).
6. J.W. Schaeffer, S. Eskinazi, J. Fluid Mech. **6**, 241 (1959).
7. S. Taneda, J. Phys. Soc. Jpn **45**, 1038 (1978).
8. P.T. Tokumaru, P.E. Dimotakis, J. Fluid Mech. **224**, 77 (1991).
9. K. Roussopoulos, J. Fluid Mech. **248**, 267 (1993).
10. R.D. Blevins, J. Fluid Mech. **161**, 217 (1985).
11. P. Huerre, P. Monkewitz, Annu. Rev. Fluid Mech. **22**, 473 (1990).
12. D. Gerich, H. Eckelmann, J. Fluid Mech. **122**, 109 (1982).
13. M. Schumm, E. Berger, P.A. Monkewitz, J. Fluid Mech. **271**, 17 (1994).
14. P. Huerre, M. Rossi, *Hydrodynamic instabilities in open flows*, in *Hydrodynamics and Nonlinear Instabilities*, edited by C. Godrèche, P. Manneville (Cambridge University Press, 1998), Chap. 2.
15. L.D. Landau, E.M. Lifshitz, *Theoretical Fluid Mechanics* (Cambridge University Press, New York, 1973).
16. P.J. Strykowski, K.R. Sreenivasan, J. Fluid Mech. **218**, 71 (1990).